Electronic Supplementary Information

Insights on the intercalation mechanism of WSe_2 onions toward metal ion capacitors: Sodium rivals Lithium

Yichun Wang[a, b▼], Xin Zhang[a, b▼], Peixun Xiong[c], Fuxing Yin[a, b], Yunhua Xu[c], Biao Wan[d, e], Qingzhou Wang[a, b], Gongkai Wang[a, b*], Puguang Ji[a, b*], Huiyang Gou[e*]

[a] *School of Material Science and Engineering, Research Institute for Energy Equipment Materials, Hebei University of Technology, Tianjin, 300130, China*

[b] *Tianjin Key Laboratory of Materials Laminating Fabrication and Interface Control Technology, Tianjin 300130, China*

[c] *School of Materials Science and Engineering, Key Laboratory of Advanced Ceramics and Machining Technology (Ministry of Education), Tianjin Key Laboratory of Composite and Functional Materials and Tianjin Key Laboratory of Molecular Optoelectronic Science, Tianjin University, Tianjin 300072, China.*

[d] *Key Laboratory of Metastable Materials Science and Technology, College of Material Science and Engineering, Yanshan University, Qinhuangdao 066004, China*

[e] *Center for High Pressure Science and Technology Advanced Research, Beijing 100094, China*

**Corresponding authors.*

E-mail addresses:

wang.gongkai@hebut.edu.cn (G. K. Wang), jipuguang@hebut.edu.cn (P. G. Ji), huiyang.gou@hpstar.ac.cn (H. Y. Gou)

▼These authors contributed equally to this work.

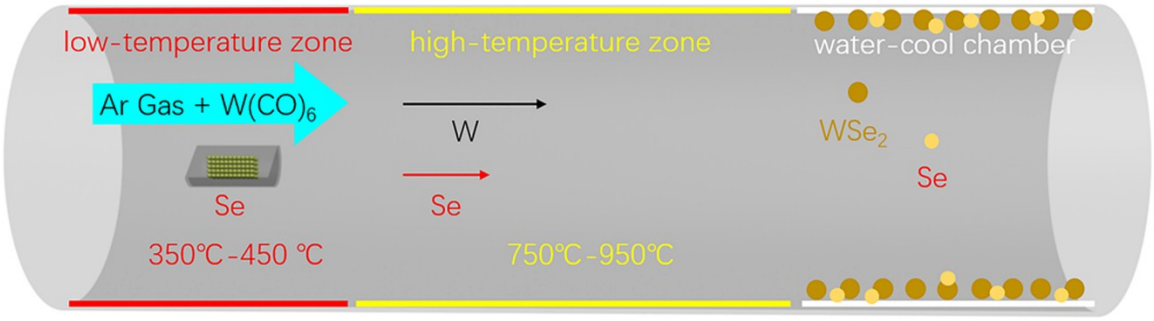

Fig. S1. Schematic illustration of the home-made CVD method for synthesis of WSe_2.

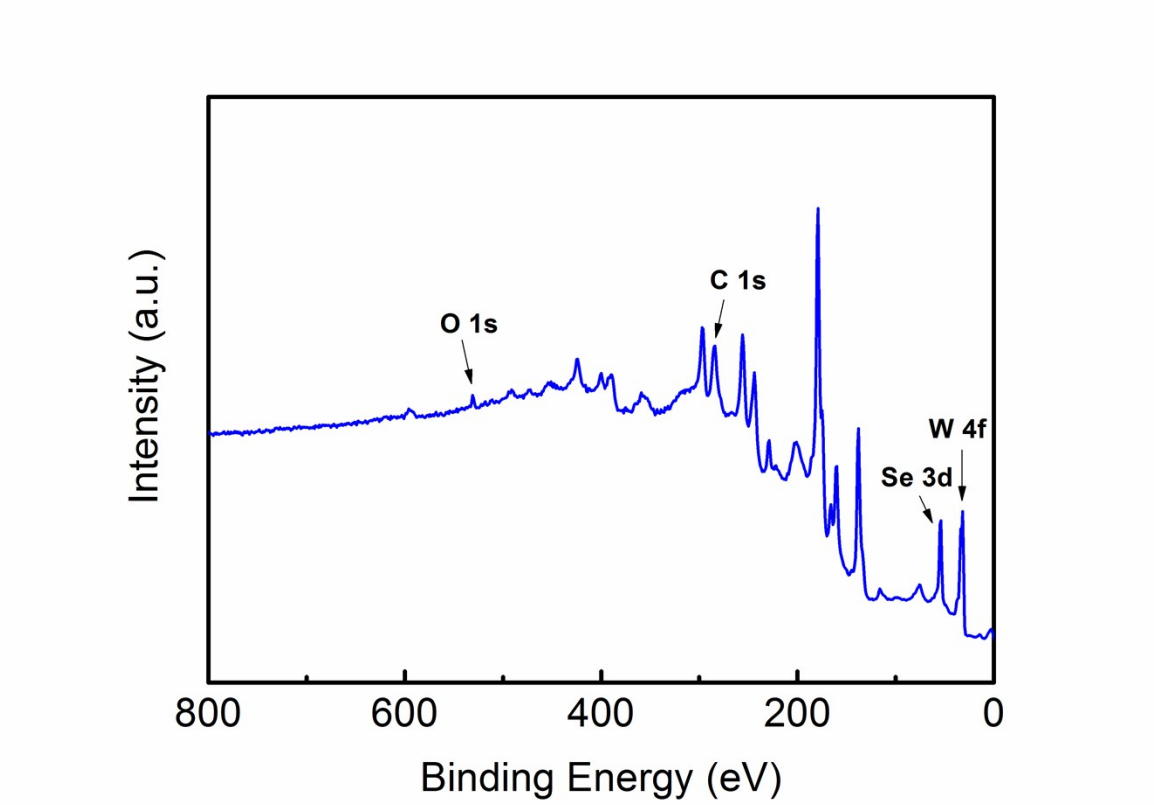

Fig. S2. XPS large survey spectrum of WSe_2.

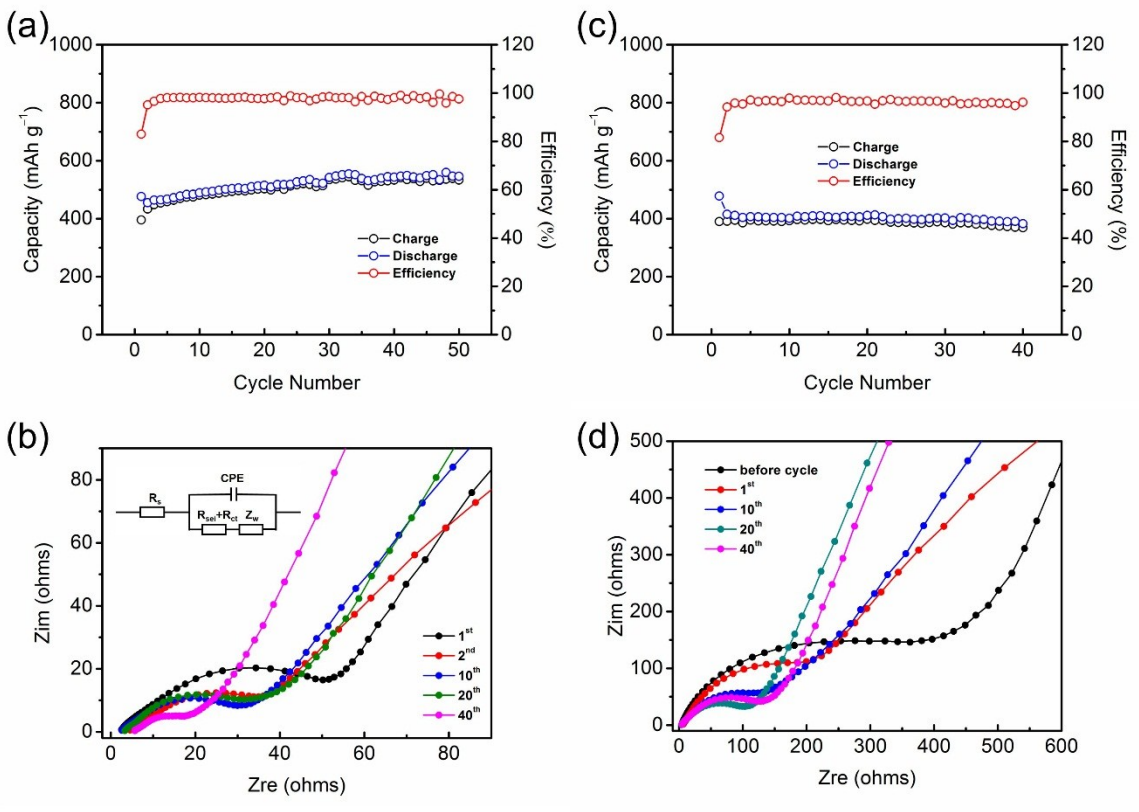

Fig. S3. Cyclic stability of WSe_2 vs (a) Lithium and (c) Sodium, and Nyquist plots of WSe_2 vs (b) Lithium and (d) Sodium.

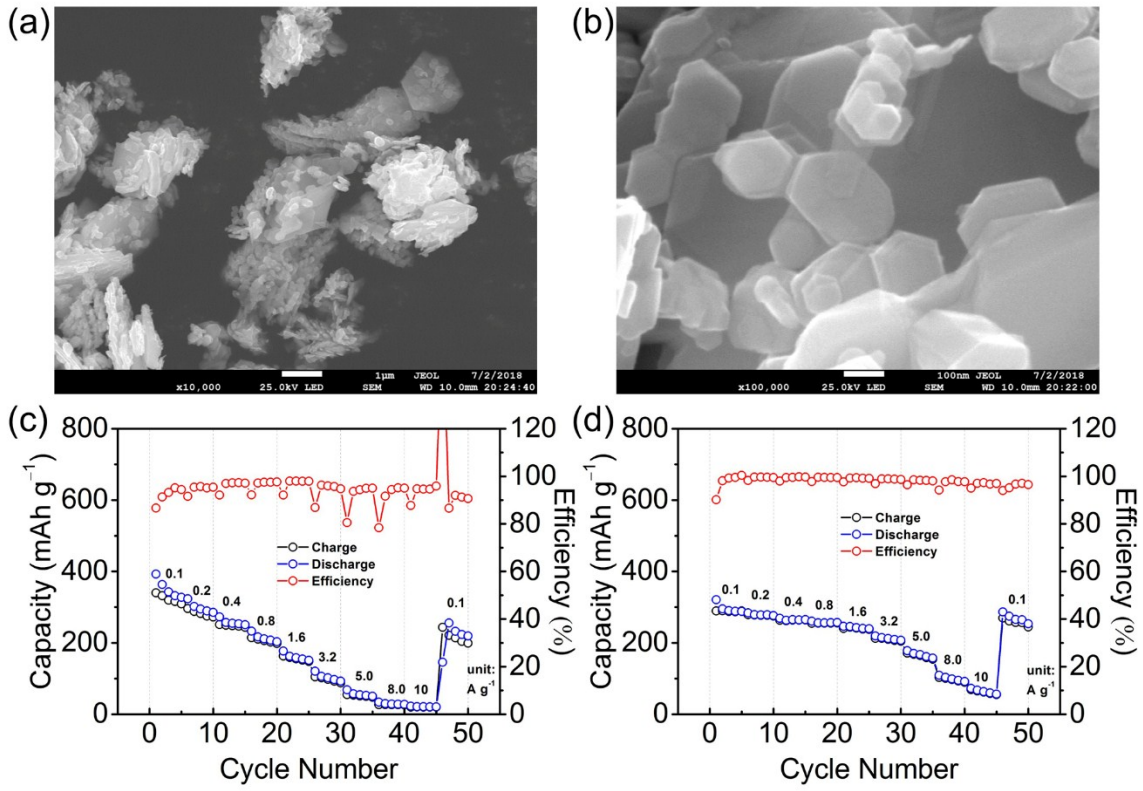

Fig. S4. (a) and (b) SEM images of commercial WSe_2, corresponding rate performances (c) vs Lithium and (d) vs Sodium.

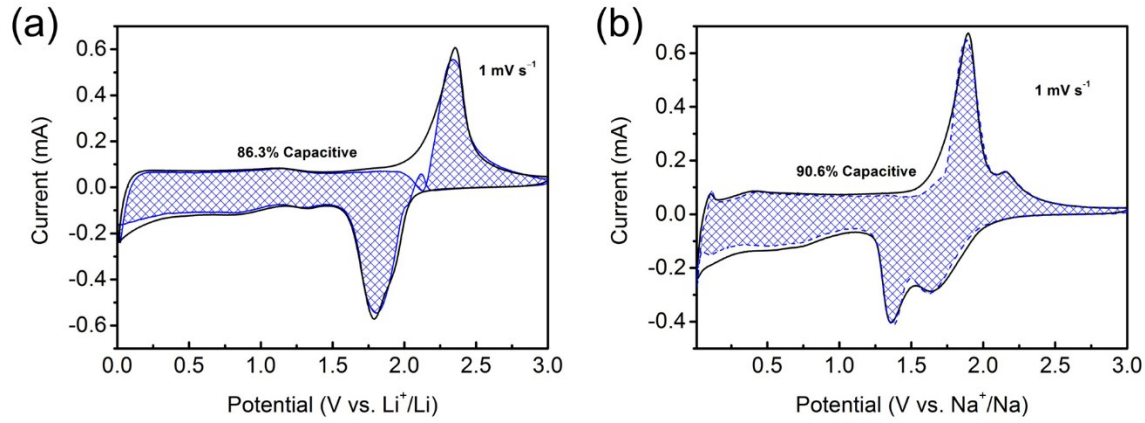

Fig. S5. (a) CV curve of WSe_2 vs Lithium at the scan rate of 1 mV s^{-1}, (b) CV curve of WSe_2 vs Sodium at scan rates of 1 mV s^{-1}, and corresponding capacitive contribution (blue region).

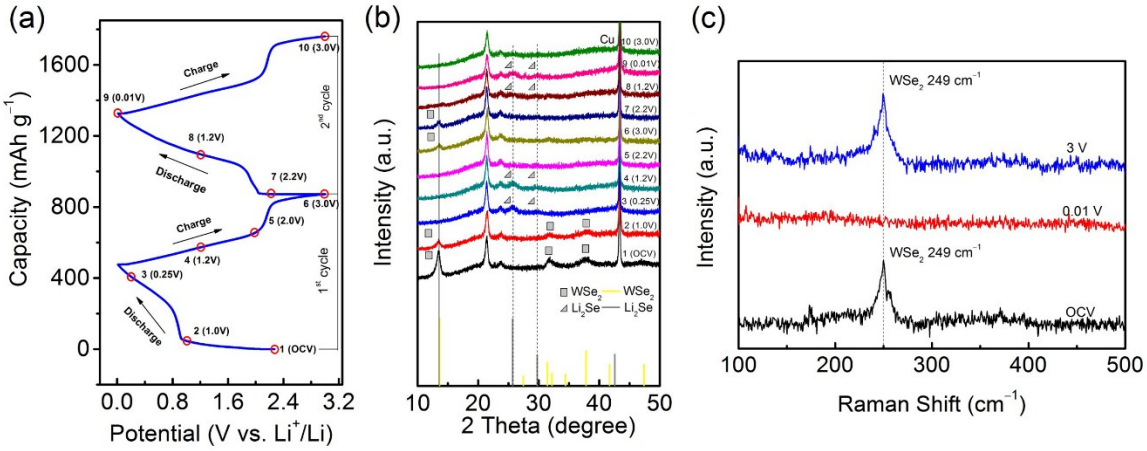

Fig. S6 Mechanism analysis of lithiation/delithiation. (a) The initial two discharge/charge curves. The numbers of one to ten refer to different potential stages corresponding to *ex situ* XRD patterns, and *ex situ* Raman spectra, (b) *ex situ* XRD patterns, (c) *ex situ* Raman spectra collected at the points of one, nine and ten.

As shown in the XRD patterns (Fig. S6a, b), at the OCV state, characteristic peaks of WSe_2 can be observed, during the initial charge process, peaks of WSe_2 disappear gradually, new diffraction peaks are assigned to the phase of Li_2Se. After the discharge process, characteristic peaks corresponding to WSe_2 can be identified again (point six and seven), indicating the recovery of WSe_2 phase. Subsequently, during the next charge/discharge cycle, the phase of Li_2Se still can be identified, indicating the reversible reaction of WSe_2 with lithium ion, while, no obvious peaks can be observed at the end of the charge process, indicating very fine structure or even amorphous phase of WSe_2 that can not be detected by XRD was obtained (The characteristic peak of WSe_2 can be identified at the point of ten in the Raman spectra in Fig.S6c, proving the recovery of WSe_2 phase). These results reveal that WSe_2 exhibits a reversible reaction with lithium ion, namely, $WSe_2 + 4Li^+ + 4e^- \leftrightarrow W + 2Li_2Se$. Specifically, during the discharge process, lithium ion intercalates with WSe_2, forming Li_2Se and W, where W is embedded in the Li_2Se matrix, namely Li_xWSe_2. Subsequently, during the charge process, lithium ion is extracted from the Li_xWSe_2 and the WSe_2 is recovered reversibly. It is worth noting that the electrochemical reaction proceeds accompany with structure refinement or amorphous phase transition of WSe_2, consistent with the previous report.[3]

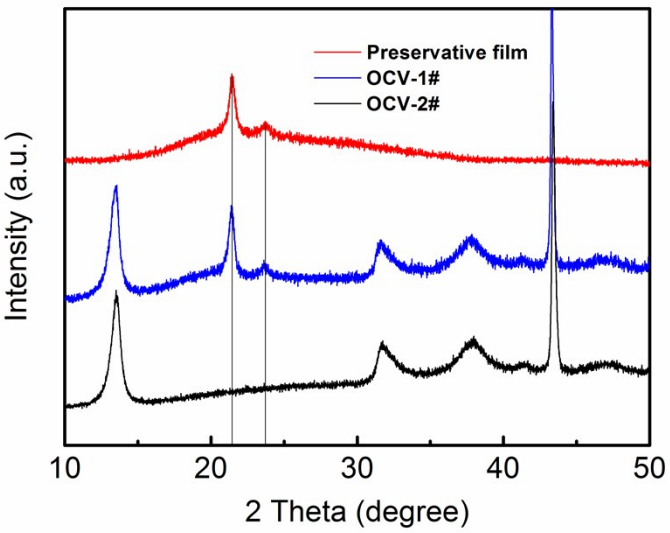

Fig. S7. *Ex situ* XRD patterns of OCV WSe_2 and the preservative film.

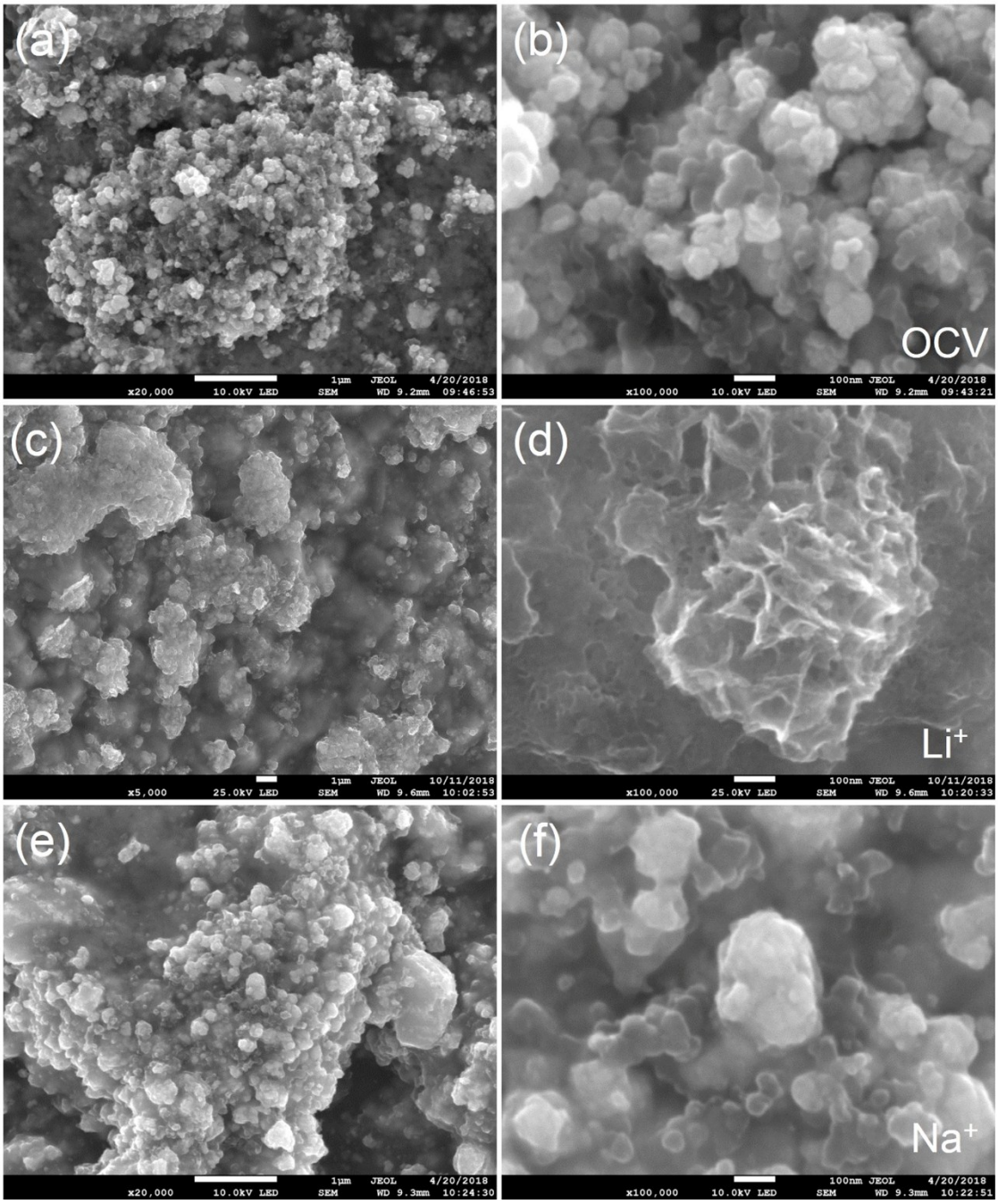

Fig. S8 SEM images of electrodes after cycles. (a, b) OCV state, (c, d) lithium ion cell, (e, f) sodium ion cell.

After the charge/discharge process, the morphology of the electrode vs sodium ion did not change a lot as compared with that at the OCV state, except the thin SEI film covered on the WSe_2 nanoparticles uniformly. Whereas, very dense SEI film with microstructure can

be observed obviously on the WSe_2 onions. These results also support the better performance of WSe_2 vs sodium ion than that vs lithium ion.

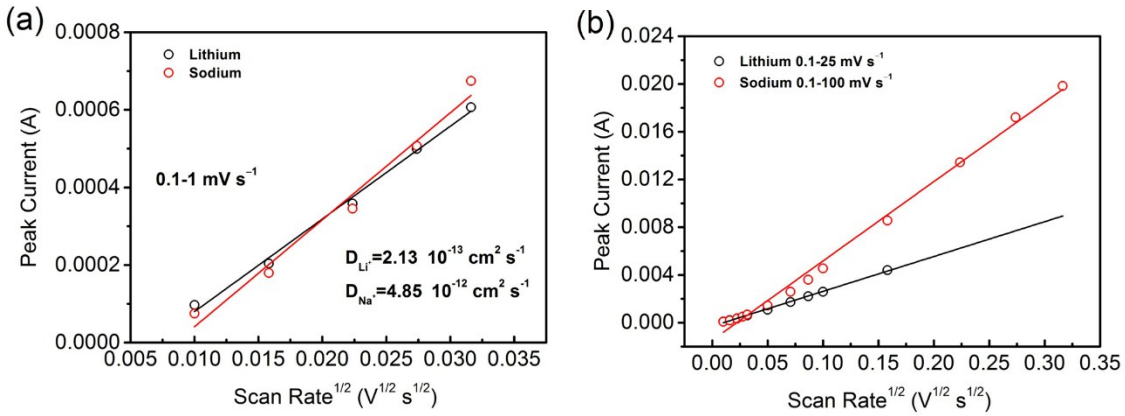

Fig. S9. Diffusion rate of lithium and sodium ion through the electrode.

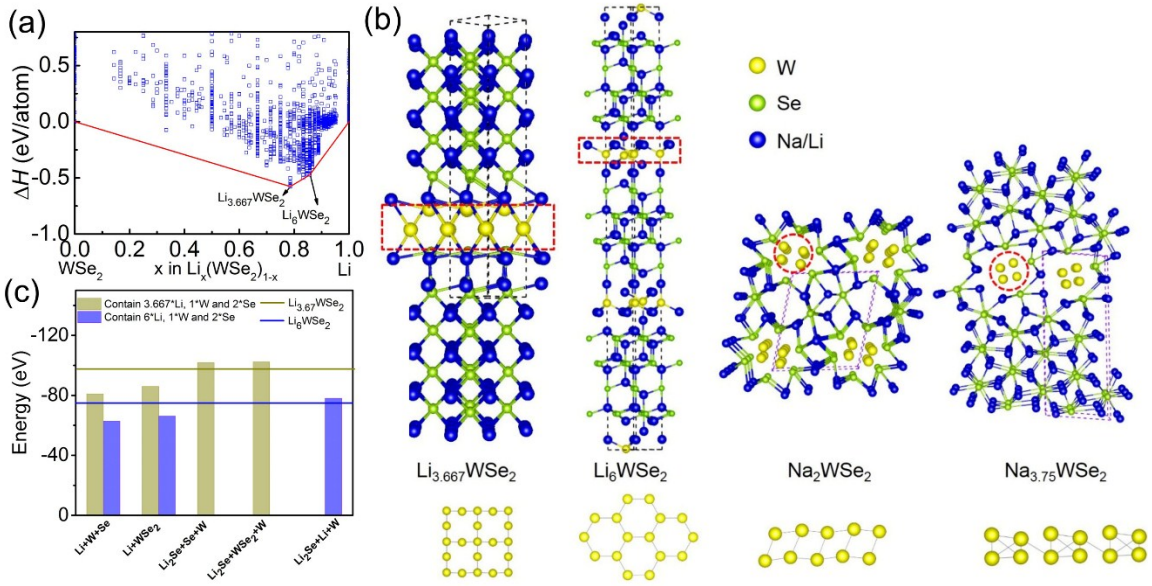

Fig. S10. (a) The calculated convex hull of $Li_x(WSe_2)_{1-x}$ for obtained candidates within the structural searching, the phases on the lines indicate its thermodynamic stability, (b) the structures of relatively stable phases of $Li_{3.667}WSe_2$ and Li_6WSe_2 as compared with $Na_x(WSe_2)_{1-x}$, in which the very different configurations can be observed, (c) the global

energy comparison of $Li_{3.667}WSe_2$ and Li_6WSe_2 with different constituent elements/compounds.

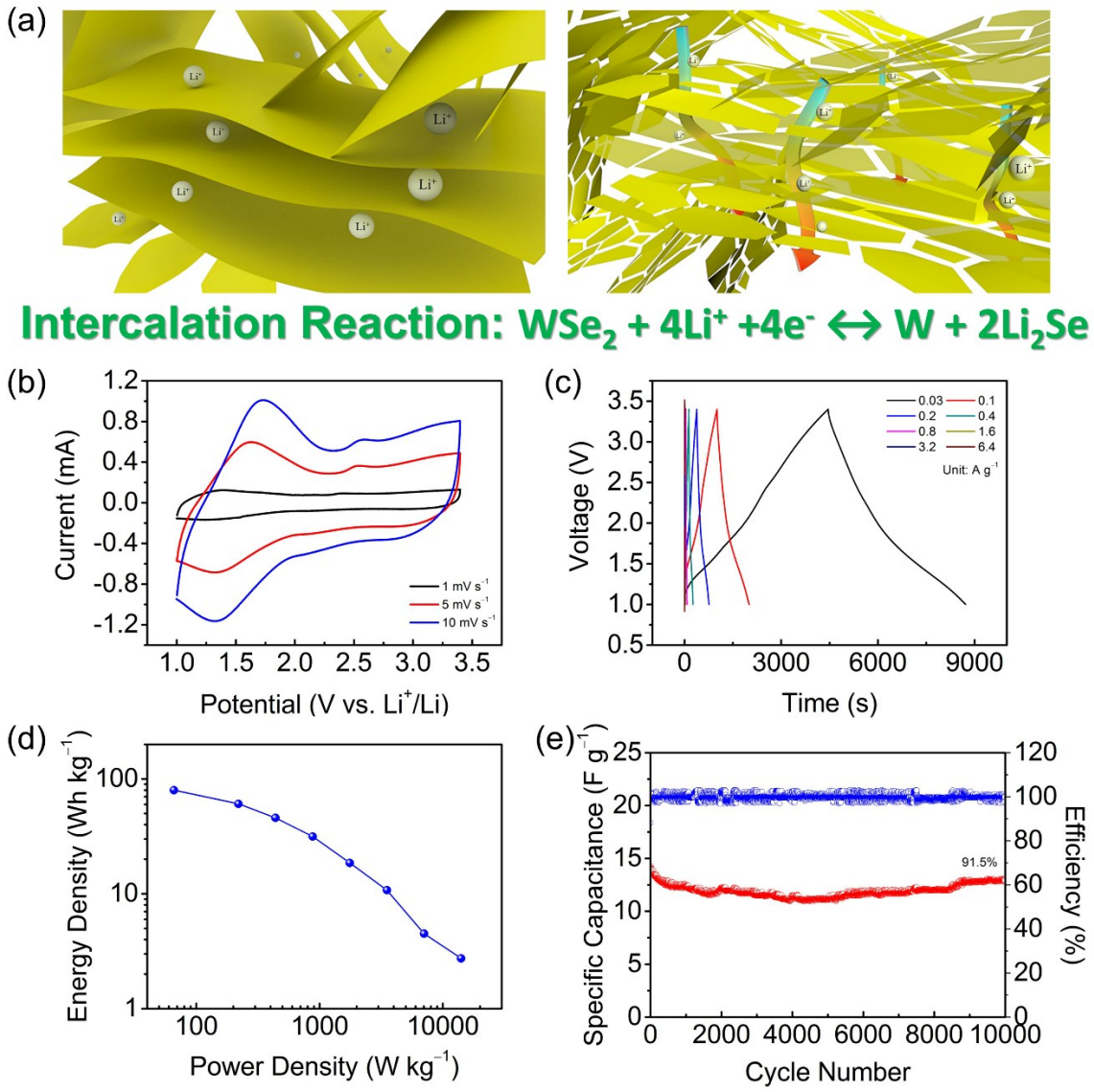

Fig. S11. (a) Schematic illustration of lithiation/delithiation mechanism, (b) CV curves and (c) galvanostatic charge/discharge profiles of LICs, (d) Ragone plots of LICs full cell based on WSe_2 anode and AC cathode, (e) cyclic stability of LICs full cell at a current density of 1000 mA h g^{-1}.

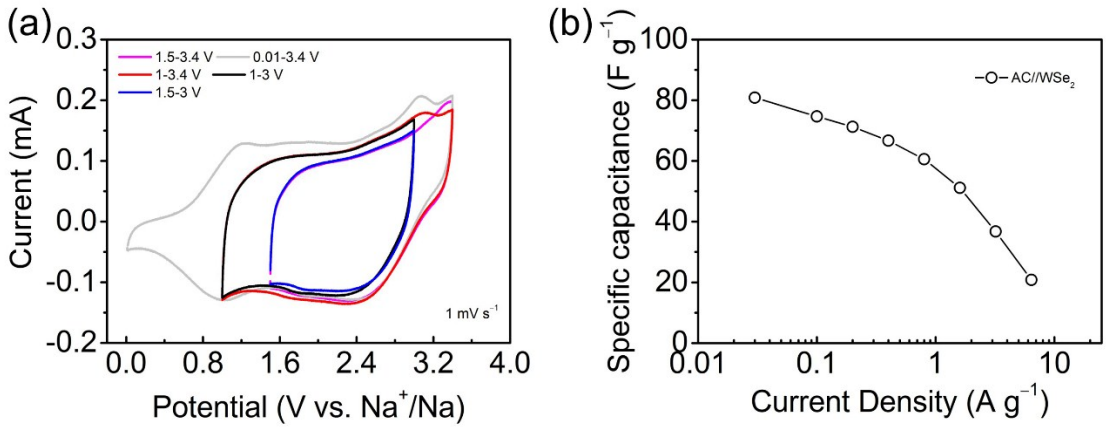

Fig. S12. (a) CV curves of SICs at various potential windows, and (b) specific capacitance at various current densities.

Table S1 Comparison of electrochemical properties with previous reports for Sodium ion anode.

Active material	Preparation	Initial coulombic efficiency	Reversible specific capacity	Rate performance	Ref.
WSe_2/C composites	high energy ball milling	58.5 %	294 mAh g^{-1} at 1 A g^{-1}	208 mAh g^{-1} at 1 A g^{-1}	1
Bulk WSe_2	Commercial	57.3 %	228 mAh g^{-1} at 0.02 A g^{-1}	130 mAh g^{-1} at 0.4 A g^{-1}	2
WSe_2 nanoplates	Solid-phase synthesis	60.3 %	450 mAh g^{-1} at 0.1 A g^{-1}	322 mAh g^{-1} at 0.8 A g^{-1}	3
MoO_2/$MoSe_2$-graphene	one-step solvothermal process	81%	404 mAh g^{-1} at 0.1 A g^{-1}	301 mAh g^{-1} at 3.2 A g^{-1}	4
WSe_2 onions	CVD	81.9%	403 mAh g^{-1} at 0.1 A g^{-1} 330 mAh g^{-1} at 0.8 A g^{-1}	309 mAh g^{-1} at 3.2 A g^{-1} 214 mAh g^{-1} at 10 A g^{-1}	This work

References

1. Zhang, Z.; Yang, X.; Fu, Y.; et al. Nanostructured WSe_2/C composites as anode materials for sodium-ion batteries. *RSC Adv*. **2016**, *6*, 12726-12729.

2. Share, K.; Lewis, J.; Oakes, L.; Carter, R. E.; Cohn, A. P.; Pint, C. L.; et al. Tungsten Diselenide (WSe_2) as a High Capacity, Low Overpotential Conversion Electrode for Sodium Ion Batteries. *RSC Adv*. **2015**, *5*, 101262-101267.

3. Yang, W.; Wang, J.; Si, C.; Peng, Z.; Zhang, Z.; et al. Tungsten diselenide nanoplates as advanced lithium/sodium ion electrode materials with different storage mechanisms. *Nano Res*. **2017**, *10*, 2584-2598.

4. Zhao, X.; Wang, H.; Yang, Y.; Neale, Z. G.; Massé, R. C.; Cao, J.; et al. Reversible and fast Na-ion storage in MoO_2/$MoSe_2$ heterostructures for high energy-high power Na-ion capacitors. *Energy Storage Materials* **2018**, *12*, 241-251.

Table S2 Bonding strength of W-W pairs of various compounds.

Compounds	W-W bond length (Å)	-ICOHP(eV/pair)
Na_2WSe_2	2.46	3.60
$Na_{3.75}WSe_2$	2.31	4.73
$Li_{3.667}WSe_2$	2.57	3.02
Li_6WSe_2	2.49	3.30